MALAYSIAN JOURNAL OF ANALYTICAL SCIENCES

Journal homepage: https://mjas.analis.com.my/

Research Article

Adsorption of allopurinol using physically activated carbon derived from *Leucaena leucocephala* branches: Optimisation and mass transfer modelling

Mohamad Hafiz Baharudin, Erniza Mohd Johan Jaya, Azrina Aziz and Mohd Azmier Ahmad*

School of Chemical Engineering, Engineering Campus, Universiti Sains Malaysia, 14300 Nibong Tebal, Penang, Malaysia

*Corresponding author: chazmier@usm.my

Received: 1 March 2026; Revised: 26 May 2026; Accepted: 27 July 2026; Published: 31 October 2026

Abstract

Allopurinol (ALLO) is increasingly reported in water bodies because conventional wastewater treatment often fails to eliminate it completely. This work prepared an activated carbon from *Leucaena leucocephala* branches (LLBAC) using a carbon dioxide (CO_2) activation route and assessed its ability to capture ALLO from water. Preparation variables were systematically optimised through response surface methodology (RSM), while Polymath mass transfer (PMT) modelling was applied to approximate the mass transfer coefficient, k_m and adsorbent surface area, a_m. The optimum synthesis conditions were 700 °C activation temperature and 1.30 h activation time, producing a removal capacity of 71.41 mg g^{-1} (actual 73.13 mg g^{-1}, error of 2.35%) with a carbon yield of 34.51% (actual 33.76%, error 2.22%). Batch adsorption experiments showed that maximum uptake occurred at 30 °C and pH 6.7, reaching 73.13 mg g^{-1}. Equilibrium behaviour followed the Freundlich model, indicating adsorption on energetically diverse surfaces with possible multilayer formation. The theoretical Langmuir monolayer capacity, Q_m was 107.96 mg g^{-1}. Kinetic results were better represented by the pseudo first order (PFO) model, suggesting that physical interactions dominated the uptake process. The surface area estimated by the Polymath model was 733.84 m^2 g^{-1}, closely agreeing with the measured mesoporous area of 800.33 m^2 g^{-1}, corresponding to a small deviation of 8.31%. Overall, the prepared LLBAC shows strong potential as an economical material for ALLO removal in water treatment.

Keywords: Adsorption process, physical activation, optimisation, isotherm, mass transfer

Introduction

Pharmaceutical substances are now widely regarded as emerging micropollutants because their presence in aquatic environments can interfere with biological systems, influence the health of aquatic plants and animals, and potentially threaten human health when they contaminate water resources. Previous research has shown that very low concentrations of these substances are sufficient to reduce water quality and gradually disturb ecological stability [1]. A large proportion, reaching about 90%, of consumed pharmaceuticals is released from the body via urine and faeces since intestinal uptake is often incomplete. These residues can subsequently reach the environment through the use of untreated sewage sludge or livestock manure, promoting their build up in agricultural wastes or their release into wastewater streams [2]. During medical use, pharmaceutical residues are commonly transferred into municipal wastewater and the sludge produced at treatment facilities. Nevertheless, many wastewater treatment plants lack the capability to effectively eliminate or transform these compounds, which allows them to remain in treated effluent and concentrate in the resulting sludge. Among the wide range of pharmaceutical products, allopurinol (ALLO), chemically known as 1,5-dihydro-4H-pyrazolo[3,4-d]pyrimidin-4-one, is widely prescribed for managing gout and is also applied in the treatment of inflammatory bowel disease, tumor lysis syndrome, certain psychiatric conditions, and cardiovascular disorders, primarily due to its effectiveness in lowering elevated uric acid levels in the bloodstream [3,4]. ALLO, which is included in the World Health Organization List of Essential Medicines, can be administered through oral or intravenous routes [5]. ALLO and its major metabolite, oxypurinol, have been detected in wastewater effluents, surface water, groundwater, and finished drinking water due to their high persistence during conventional wastewater treatment processes [6]. ALLO has been associated with severe adverse reactions, including Stevens–Johnson syndrome and toxic epidermal necrolysis, in susceptible individuals [7,8]. Although limited studies have specifically evaluated the adverse effects of ALLO in aquatic environments, the persistent

occurrence of ALLO and oxypurinol in wastewater and water systems remains concerning due to the possibility of prolonged environmental exposure.

Numerous technologies have been employed to eliminate pharmaceutical compounds from wastewater, each offering distinct advantages and limitations. Among these, adsorption which relies on the surface interaction mechanism, has emerged as a particularly effective method due to its versatility in capturing a wide range of contaminants, including heavy metals [9,10], antidiabetic drug [11], chlorinated hydrocarbon [12], pharmaceutical compounds [13], synthetic dyes [14,15] and others. This method is favoured for its straightforward operation, high removal efficiency, and economic viability. Traditionally, the activated carbon (AC) used in adsorption is sourced from coal, a non-renewable material associated with environmental concerns and high production costs. In response, researchers are increasingly turning to agricultural byproducts such as *alpinia galanga* stem [16], sludge biomass [17], Tecoma chip wood [18] and others. *Leucaena leucocephala* represents an abundant agricultural residue source and is a fast-growing tropical tree from the Fabaceae family, originally native to southern Mexico and Central America. It thrives in warm climates with sufficient rainfall and is characterized by dense and extensive branching [19]. Outside its native habitat, the species has been broadly cultivated in plantation programs throughout Malaysia, Indonesia, Papua New Guinea, and other Southeast Asian countries, and later spread during the 19th century to areas including Hawaii, Australia, India, parts of Africa, and the Caribbean [19]. In the Malaysian context, this plant is classified as an invasive species [20]. Converting its branches into activated carbon (AC) provides a practical and environmentally sound approach for controlling its spread while creating value added materials. Unlike many previously reported biomass-based AC studies that primarily focus on adsorption performance alone, the present work combines sustainable utilization of an invasive species with statistical optimisation and advanced mass transfer modelling to provide a more comprehensive understanding of the adsorption mechanism. Furthermore, the incorporation of the Polymath mass transfer (PMT) simulation enables simultaneous evaluation of transport behaviour and adsorbent surface area prediction, which remains rarely explored in biomass derived AC investigations.

AC remains one of the most widely applied adsorbents in wastewater treatment due to its high surface area, well developed pore structure, strong adsorption capability, and relatively simple operation. Although other emerging technologies such as biochar, metal organic frameworks (MOFs), graphene-based materials, advanced oxidation processes (AOPs), and membrane filtration have demonstrated promising performance for pharmaceutical removal, each technology possesses certain limitations. Biochar generally exhibits lower surface area and adsorption capacity compared to AC, which may restrict its removal efficiency for contaminants. Additionally, biochar often requires further activation to enhance its adsorption properties [21]. MOFs are porous materials consisting of metal nodes and organic ligands that exhibit high porosity, large surface area, and tunable surface chemistry. Despite these advantages, their industrial application remains limited due to high production cost, low selectivity in pollutant mixtures, recycling difficulties, and stability concerns [22]. Graphene and its derivatives are among the most advanced carbonaceous adsorbents due to their high surface area, excellent chemical stability, enhanced active sites, and large delocalised π electron system, making them highly effective for wastewater treatment [23]. However, their practical application remains limited by expensive synthesis methods, poor scalability, and low reproducibility for large scale production [24]. Pharmaceuticals in wastewater are not easily degraded by conventional treatment technologies. Advanced AOPs have emerged as a promising alternative for the degradation of these compounds at trace levels [25]. However, their practical application is often limited by high operational cost and energy consumption, which reduce their overall cost effectiveness [26]. Membrane technology offers high separation efficiency and high quality permeate production. However, membrane fouling, high operational cost, energy consumption, and skilled maintenance requirements remain major limitations [27].

This study concentrates on converting *Leucaena leucocephala* branches into AC designated as LLBAC and on refining the preparation conditions using response surface methodology (RSM). This approach is selected because it lowers the number of required experiments while still allowing strong statistical assessment and dependable optimisation of processing factors [28]. Enhancement of AC production has attracted increasing interest since its performance depends on numerous influencing parameters. RSM serves as an effective statistical framework for handling several variables simultaneously and for describing process behaviour with greater accuracy [29]. Within RSM, the central composite design (CCD) is frequently applied as it limits the total experimental trials, clarifies interactions among factors, and supports the development of predictive equations. Three dimensional response plots are used to visualise the influence of variables, whereas analysis of variance (ANOVA) is applied to confirm model validity and statistical significance [30]. AC removes pollutants through its extensive surface area and the presence of reactive sites. Achieving higher porosity commonly demands elevated temperatures, prolonged treatment periods, and additional reagents,

which raise operational expenses. To address these limitations, a physical activation route with carbon dioxide (CO_2) as the gasifying medium is adopted. This strategy eliminates separate chemical treatment steps, thereby improving time, energy, and resource efficiency while maintaining the adsorption capability of the produced AC [31]. Furthermore, physically activated AC has been proven to be effective for the adsorption of various pharmaceutical adsorbates. For instance, *chontaduro* seed based AC successfully adsorbed 240.70 mg/g of ibuprofen [32], while *Astragalus mongholicus* based AC successfully adsorbed 46.83 mg/g of diclofenac [33]. These findings demonstrate that physically ACs possess promising adsorption capability for pharmaceutical removal without requiring chemical activating agents.

The novelty of this study lies in utilising the Polymath mass transfer model to evaluate adsorption capacity. Traditional kinetic approaches such as the pseudo-first order (PFO) and pseudo-second order (PSO) models yield only a single overall rate constant, even though adsorption proceeds through three consecutive steps: external film transport, intraparticle movement, and attachment at surface sites. Of these steps, pore diffusion is commonly assumed to be fast and is frequently disregarded [34]. Classical transport and diffusion models, including the intraparticle diffusion model and Boyd analysis, have been widely employed to evaluate adsorption transport mechanisms and rate controlling steps in porous adsorbents. These established models provide valuable qualitative insight into diffusion behaviour; however, each model individually describes only specific transport aspects of the adsorption process. To overcome this limitation, the present study employed the pore and surface diffusion model (PMT) to analyse the kinetic behaviour of ALLO adsorption onto LLBAC. Therefore, the PMT model was not intended to replace conventional diffusion models, but rather to complement them by providing simultaneous evaluation of both external film transfer and intraparticle pore diffusion parameters. Unlike conventional kinetic models such as PFO and PSO, which mainly describe adsorption rate trends, the PMT model enables quantitative evaluation of both the external film mass transfer coefficient and intraparticle pore diffusion parameter. This provides deeper mechanistic insight into the controlling adsorption pathways and transport behaviour within the porous adsorbent structure. Furthermore, the PMT simulation permits estimation of the effective surface area of LLBAC based on mass transfer characteristics, allowing indirect comparison with the surface properties commonly reported ACs. The estimated transport and surface parameters obtained for LLBAC demonstrated competitive diffusion behaviour relative to previously reported commercial AC systems. The PMT model was originally proposed by [35], and subsequently refined by [30] and [36] to improve the correlation between experimental adsorption data and calculated mesoporous surface area values. Collectively, this strategy integrates sustainable biomass conversion, preparation optimisation, and detailed mass transfer analysis to establish a robust platform for effective ALLO removal using LLBAC, contributing to improved environmental protection and wastewater treatment practices.

Materials and Methods

Precursor, chemicals, and gases

Leucaena leucocephala branches were collected from a roadside secondary vegetation area in Penang, Malaysia. ALLO (pharmaceutical secondary standard, synthetic powder, ≥ 99 % purity by thin-layer chromatography) was obtained from Sigma-Aldrich for use in this study. The molecular formula, molecular weight, and purity of allopurinol are $C_5H_4N_4O$, 136.11 g mol^{-1}, and ≥ 99 %, respectively. Hydrochloric acid (HCl, 37 % concentration) and sodium hydroxide (NaOH, 98 % purity), employed for pH regulation, were sourced from the same supplier. For the multicomponent adsorption experiments, potassium nitrate (KNO_3; 99.0% purity), lead(II) nitrate ($Pb(NO_3)_2$; 99.0% purity), and paracetamol (PARA, $C_8H_9NO_2$; 98.0% purity) were obtained from Sigma-Aldrich. High purity carbon dioxide gas (CO_2, 99.70 %) and nitrogen gas (N_2, 99.90%), utilised as both the activating and inert atmosphere gas, was provided by MOX Gases Berhad, Malaysia.

Synthesis of LLBAC

The precursor was dried in an oven at 60 °C for 48 h to remove residual moisture. The dehydrated material was subsequently transferred into a vertical furnace and subjected to activation under a CO_2 stream at a flow rate of 150 cm^3 min^{-1}. For RSM-based optimisation, activation trials were performed at 400, 550, and 700 °C with holding durations of 1, 2, and 3 h, as summarised in **Table 1**. Once the optimum preparation conditions were established, LLBAC was produced at 700 °C for 1.30 h. After activation, the sample was cooled to ambient temperature while maintaining the CO_2 atmosphere before being taken out of the furnace. The final solid obtained was designated as LLBAC. The production yield of LLBAC was determined using the following expression.:

$$Yield\ (\%) = \frac{W_{LLBAC}}{W_{precursor}} \quad (1)$$

where W_{LLBAC} refers to the weight of LLBAC and $W_{precursor}$ refers to the weight of dry *Leucaena leucocephala* branches.

Optimisation investigation

For optimisation purposes, the experimental results were processed using Design Expert software (version 12, Stat Ease Inc., Minneapolis, USA). A RSM scheme

employing a CCD was utilised to evaluate the effects of two preparation factors, specifically activation temperature (X_1) and activation duration (X_2). Two responses were considered, namely ALLO adsorption capacity (Y_1) and LLBAC yield (Y_2). The studied factors were assigned three coded levels of −1, 0, and +1, representing activation temperatures of 400, 550, and 700 °C and activation times of 1, 2, and 3 h, respectively. The suggested optimum settings were confirmed by limiting the variables to the selected experimental range and setting both responses to be maximised within the Design Expert program, which allowed assessment of the model's predictive accuracy.

Characterisation methods

The synthesised samples were comprehensively characterised to evaluate their physicochemical attributes, including specific surface area determined by the Brunauer–Emmett–Teller approach, mesoporosity, total pore volume, and pore size distribution. These textural characteristics were measured using a Micromeritics ASAP 2010 adsorption–desorption analyser. Elemental composition was analysed with a PerkinElmer Series II 2400 instrument (USA). The zeta potential analysis was conducted using a Zetasizer Nano Series instrument provided by DKSH.

Adsorption isotherm investigation

Batch adsorption tests were conducted to evaluate the equilibrium characteristics of ALLO uptake by LLBAC. Six Erlenmeyer flasks were prepared, each containing 200 mL of ALLO solution with initial concentrations (C_o, mg L^{-1}) of 10, 20, 40, 60, 80, and 100 mg L^{-1}, and the suspensions were shaken in a thermostatic water bath at 30 °C until equilibrium was reached. The selected temperature represents typical ambient conditions in tropical wastewater systems and is widely used in adsorption investigations to enable comparison. The adsorbent loading (W) was maintained at 0.20 g for each flask. The equilibrium concentration of ALLO (C_e, mg L^{-1}) was measured at 250 nm with a UV–Vis spectrophotometer (Agilent Cary 60, USA). The equilibrium adsorption capacity (q_e, mg g^{-1}) was subsequently determined using the following equation:

$$q_e = \frac{(C_o - C_e)V}{W} \quad (2)$$

The experimental data were inspected with several models, and the corresponding equations for each model are described by the following equations:

Langmuir [37]:

$$q_e = \frac{Q_m K_L C_e}{1 + K_L C_e} \quad (3)$$

Freundlich [38]:

$$q_e = K_F C_e^{1/n_F} \quad (4)$$

Temkin [39]:

$$q_e = \frac{RT}{B}\ln(AC_e) \quad (5)$$

The parameters associated with these isotherm models have been thoroughly described in the study reported by [40].

Adsorption kinetic investigation

Batch adsorption results were utilised to assess kinetic behaviour through two commonly applied models, namely the pseudo first order (PFO) and pseudo second order (PSO) rate expressions. These models were analysed using the corresponding mathematical relationships shown below, allowing systematic evaluation of adsorption trends, rate controlling steps, and potential diffusion contributions. The kinetic assessment offered valuable understanding of the interactions between ALLO molecules and the prepared LLBAC, and further clarified the kinetic pathways and controlling factors that determine adsorption efficiency in aqueous systems:

PFO [41]:

$$q_t = q_e[1 - exp(-k_1 t)] \quad (6)$$

PSO [41]:

$$q_t = \frac{k_2 q_e^2 t}{1 + k_2 q_e t} \quad (7)$$

The parameters related to these kinetic equations have been comprehensively reported and clearly described in the previous study cited in [42], offering useful reference and context for their proper interpretation in the present work.

Adsorption mechanism and mass transfer investigatio

To obtain further understanding of the adsorption mechanism and identify the possible rate controlling step, the Weber–Morris intraparticle diffusion model [43] together with the Boyd diffusion analysis [44] were applied. The related equations are given below, respectively:

$$q_t = k_i t^{0.5} + C_i \quad (8)$$

$$B_t = -0.4977 - \ln\left(1 - \frac{q_t}{q_e}\right) \quad (9)$$

where k_i is the intraparticle diffusion rate constant (mg/g. $h^{1/2}$), C_i rrepresents the boundary layer thickness constant, and B_t is the Boyd number. In

addition to these classical diffusion models, the Polymath mass transfer (PMT) model was also applied to further evaluate the adsorption mass transfer behaviour. The PMT model was applied through Polymath software (version 6.2, USA) to estimate important mass transfer parameters and to project the adsorption surface area of LLBAC. The fundamental equations describing the PMT model are given below [30,36]:

$$C = C_e - (C_e - C_0)\exp[-t(k_{PMT} + a_m k_m)] \quad (10)$$

where k_{PMT} is PMT's rate constant (h^{-1}), k_m is the coefficient of film diffusion ($mg.m.L^{-1}h^{-1}$) and a_m is the adsorbent surface area ($m^2\ g^{-1}$).

Adsorption thermodynamic investigation

Temperature variation plays a significant role in determining the efficiency of the adsorption process. Therefore, a thermodynamic investigation was performed to evaluate the changes in enthalpy (ΔH°), entropy (ΔS°), Gibbs free energy (ΔG°), and Arrhenius activation energy (E_a), expressed in kJ/mol, kJ/mol·K, kJ/mol, and kJ/mol, respectively. The values of ΔH° and ΔS° were obtained using the Van't Hoff equation shown below:

$$ln\ K_c = \frac{\Delta S°}{R} - \frac{\Delta H°}{RT} \quad (11)$$

where K_c (dimensionless) is computed using the following equation [45]:

$$K_c = \frac{1000\frac{mg}{g} \times K_L \times molecular\ weight\ of\ adsorbate \times [adsorbate]^{\circ}}{\gamma} \quad (12)$$

where [adsorbate]° estimated at 1 mol/L (standard state); ϒ denotes the activity of the adsorbate (dimensionless); and K_L is the Langmuir constant (L/mg). Other thermodynamic parameters were calculated via the following equation:

$$\Delta G° = \Delta H° - T\Delta S° \quad (13)$$

$$ln\ k_2 = ln\ A - \frac{E_a}{RT} \quad (14)$$

where A denotes the Arrhenius factor. All adsorption experiments were conducted in triplicate, and the reported values represent the mean ± standard deviation (SD). Error bars shown in the adsorption plots correspond to one standard deviation from three independent measurements.

Adsorption in multicomponent system investigation

Multicomponent adsorption experiments were conducted to investigate the competitive behaviour between ALLO and coexisting species under binary and quaternary conditions using LLBAC, with the aim of simulating a realistic hospital wastewater matrix. All adsorption tests were performed at a constant temperature of 30 °C under the natural pH of the solutions without further adjustment. For the single component system, 0.20 g of LLBAC was added into 200 mL of solution. In the binary system, 0.40 g of adsorbent was introduced into 400 mL of solution, whereas the quaternary system employed 0.80 g of LLBAC in 800 mL of solution. The initial concentration of each adsorbate was maintained at 100 mg/L throughout the study. ALLO, paracetamol (PARA), nitrate (NO_3^-), and lead (Pb^{2+}) were selected as representative coexisting substances for the adsorption evaluation.

PARA was utilised directly without further treatment, while potassium nitrate (KNO_3) and lead(II) nitrate ($Pb(NO_3)_2$) were used as the sources of NO_3^- and Pb^{2+} ions, respectively. Binary adsorption studies were carried out by pairing ALLO individually with PARA, NO_3^-, or Pb^{2+}, with both components present at equal initial concentrations of 100 mg/L. In the quaternary system, ALLO, PARA, NO_3^-, and Pb^{2+} were simultaneously introduced at identical concentrations to mimic the complex composition and competitive interactions commonly encountered in actual hospital wastewater. The adsorption performance of each system was monitored over time until equilibrium conditions were attained. All adsorption and optimisation experiments were conducted in triplicate to ensure the reliability, reproducibility, and accuracy of the obtained results.

Results and Discussion

Optimisation process

Regression model development

Table 1 summarizes the experimental design employed for producing optimised LLBAC. A face-centred central composite design (CCD) consisting of four factorial points, four axial points (*), and five replicated centre points (*) was employed to evaluate the effects of activation temperature and activation duration on ALLO uptake and LLBAC yield. The replicated centre points were incorporated to estimate pure experimental error and assess experimental reproducibility. The measured ALLO uptake varied from 43.45 to 88.75 mg g^{-1}, while the corresponding LLBAC yield was recorded within the range of 22.85 to 42.52 %. The results compiled in this table were used to establish empirical model equations, conduct analysis of variance, and generate three-dimensional response surface plots to clarify the interactions between preparation variables and the evaluated responses.

Table 1. Variables and responses for LLBAC production as generated by the RSM

Run	Cu^{2+}-SSAC preparation variables		Responses	
	Activation temperature, X_1 (°C)	Activation time, X_2 (h)	ALLO uptake, Y_1 (mg/g)	LLBAC yield, Y_2 (%)
*1	400	2	57.11	39.52
**2	550	2	66.61	27.19
**3	550	2	64.14	26.19
4	400	3	58.42	39.62
**5	550	2	62.63	25.11
**6	550	2	65.52	26.87
*7	550	3	74.21	24.12
*8	550	1	49.16	28.56
9	700	1	67.41	37.21
10	400	1	43.45	42.52
**11	550	2	63.96	25.89
12	700	3	88.75	22.85
*13	700	2	80.85	30.11

*axial points; **centre points

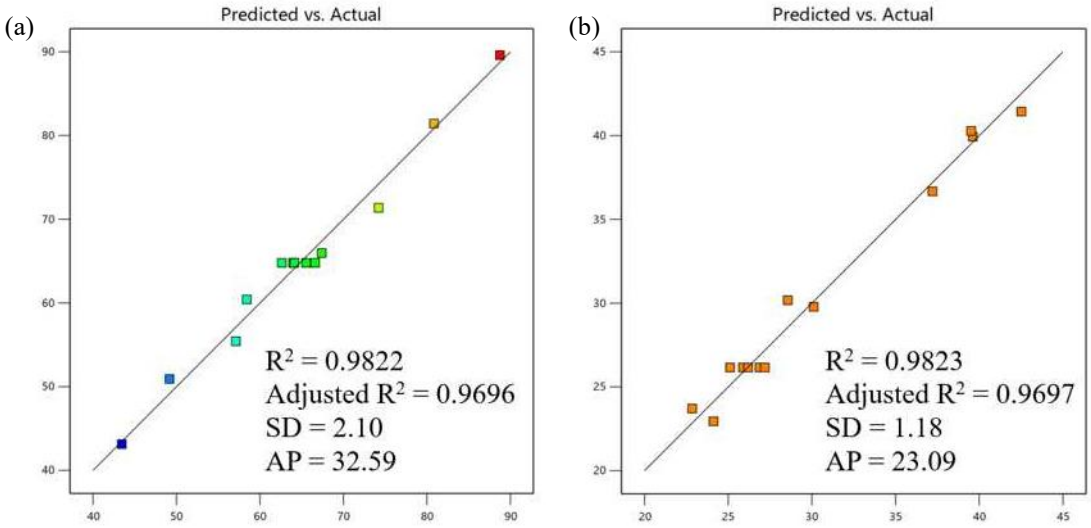


Figure 1. Plots of predicted versus actual for (a) ALLO uptakes and (b) LLBAC yield responses

The quadratic models formulated in coded variables showed high predictive performance for the two response parameters, namely ALLO adsorption capacity (Y_1) and LLBAC yield (Y_2), as detailed in Equations (9) and (10), respectively:

ALLO uptake (mg/g), Y_1

$$Y_1 = 64.79 + 13.00X_1 + 10.23X_2 + 1.59X_1X_2 + 3.64X_1^2 - 3.65X_2^2 \quad (15)$$

LLBAC yield (%), Y_2

$$Y_2 = 26.16 - 5.25X_1 - 3.62X_2 - 2.86X_1X_2 + 8.88X_1^2 + 0.4014X_2^2 \quad (16)$$

In RSM applications, quadratic models are frequently employed because they can represent curvature in experimental responses. In contrast to linear approaches that assume a direct proportional relationship between variables and outcomes, quadratic models include squared and interaction components. The inclusion of these components allows a richer representation of nonlinear trends and interrelated factor effects. Consequently, quadratic models are highly appropriate for optimisation studies since they permit concurrent evaluation of main effects, factor interactions, and higher order contributions to the observed responses [30].

Figure 1 shows the plots of predicted versus actual for (a) ALLO uptakes and (b) LLBAC yield. The ALLO adsorption response exhibited R^2 and adjusted R^2 values of 0.9822 and 0.9696, while the LLBAC yield showed similarly high values of 0.9823 and 0.9697. Such elevated and closely matched values indicate that the fitted models possess strong explanatory power and successfully represent the variability observed in the experimental data. Furthermore, the small standard deviations (SD), measured at 2.10 for ALLO uptake and 1.18 for LLBAC yield, indicate that the predicted outputs closely follow the experimental

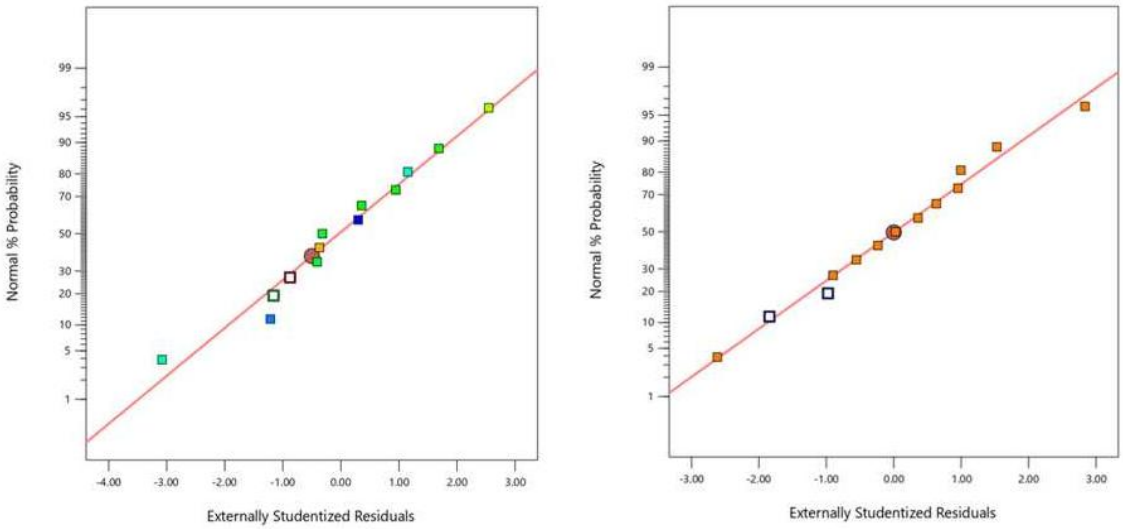


Figure 2. Normal plots of residual for (a) ALLO uptakes and (b) LLBAC yield responses

Table 2. ANOVA results for ALLO uptake and LLBAC yield responses

Source	Response 1, Y_1 (mg/g): ALLO uptakes by LLBAC				
	Sum of the Squares	**DF**	**Mean Square**	**F Value**	**p-value**
Model	1705.65	5	341.13	77.45	< 0.0001
X_1	1014.78	1	1014.78	230.41	< 0.0001
X_2	627.51	1	627.51	142.48	< 0.0001
X_1X_2	10.14	1	10.14	2.30	0.1729
X_1^2	36.65	1	36.65	8.32	0.0235
X_2^2	36.84	1	36.84	8.37	0.0232
Lack of fit	21.45	3	7.15	3.05	0.1150
Source	**Response 2, Y_2 (%): LLBAC yield**				
	Sum of the Squares	**DF**	**Mean Square**	**F Value**	**p-value**
Model	540.43	5	108.09	77.80	< 0.0001
X_1	165.27	1	165.27	118.96	< 0.0001
X_2	78.48	1	78.48	56.49	0.0001
X_1X_2	32.83	1	32.83	23.63	0.0018
X_1^2	217.61	1	217.61	156.63	< 0.0001
X_2^2	0.4450	1	0.4450	0.3203	0.5891
Lack of fit	7.02	3	2.34	3.47	0.1304

measurements, demonstrating consistent prediction quality. The adequate precision (AP) ratios reached 32.59 for ALLO uptake and 23.09 for LLBAC yield. Because these ratios are far greater than the recommended minimum of 4, the models exhibit a pronounced signal compared with background noise. This confirms that the proposed equations are dependable for predicting responses throughout the investigated design range [46].

Figure 2 illustrates the normal probability plots of residuals for (a) ALLO uptakes and (b) LLBAC yield responses. The residual points for both responses were distributed in close proximity to the straight reference line without severe deviation or irregular scattering patterns. This behaviour indicates that the residuals were approximately normally distributed, suggesting that the assumptions underlying the quadratic regression models were reasonably satisfied. In addition, the absence of pronounced outliers and systematic curvature implies that no substantial abnormal experimental error or model inadequacy was present within the investigated design range. The relatively linear arrangement of the residual points further supports the reliability and statistical validity of the developed RSM models for describing the adsorption and yield responses.

Analysis of variance (ANOVA)

Table 2 presents the ANOVA outcomes for ALLO adsorption and LLBAC yield, showing that both fitted quadratic equations are highly significant, with probability values well below 0.0001. For the ALLO response, activation temperature (X_1) and activation

duration (X_2) emerged as influential linear factors, while the squared terms X_1^2 and X_2^2 were also meaningful, revealing noticeable curvature in the response surface. The magnitude of the F statistics identifies activation temperature as the most influential variable for ALLO removal (F = 230.41), with activation time contributing to a lesser but still important extent (F = 142.48). In the case of LLBAC yield, statistical relevance was detected for activation temperature, activation time, their combined effect (X_1X_2), and the squared temperature term (X_1^2). Temperature again showed the strongest effect on yield (F = 118.96), whereas time played a supportive role (F = 56.49).

Furthermore, the lack-of-fit tests for both ALLO uptake and LLBAC yield were statistically insignificant ($p > 0.05$), indicating that the developed quadratic models adequately represented the experimental data within the investigated design space. The insignificant lack-of-fit also suggests that the residual variation was primarily associated with random experimental error rather than systematic model inadequacy. Taken together, these ANOVA findings highlight activation temperature as the principal parameter controlling both adsorption performance and carbon yield.

Three-dimensional (3D) surface plot

Figure 3 depicts the three-dimensional (3D) response plots that portray how activation temperature and activation duration jointly influence (a) ALLO adsorption and (b) LLBAC yield. As observed in **Figure 3(a)**, the highest ALLO removal, reaching 84.25 mg g^{-1}, occurred at 700 °C with a 3 h treatment period, indicating a clear cooperative effect between temperature and time. Raising the temperature from 400 to 700 °C consistently elevated ALLO uptake within the tested time window of 1 to 3 h. This trend is linked to more effective thermal treatment, which enhances volatile release, pore formation, and surface development, thereby improving adsorption performance [47]. Simultaneously, the breakdown of light hydrocarbon fractions promotes greater carbon enrichment and clearer pore structure formation [48]. Nevertheless, although the highest adsorption capacity was achieved at 700 °C and 3 h, this condition simultaneously produced the lowest LLBAC yield, indicating that maximum adsorption performance did not correspond to the most balanced overall process condition.

Conversely, **Figure 3(b)** shows that the minimum LLBAC yield, 22.85%, was recorded under the most severe condition of 700 °C for 3 h, revealing that harsh activation reduces solid recovery. Increasing temperature from 400 to 700 °C intensified pyrolytic reactions, causing greater elemental depletion and lowering product yield [30]. Extending the heating period further aggravated this decline, especially at high temperatures, because sustained thermal exposure accelerates structural decomposition and mass loss [49]. This behaviour demonstrates the existence of competing response tendencies, where conditions favouring maximum adsorption capacity may adversely affect carbon yield. These observations emphasize that activation temperature and activation time must be carefully balanced to secure satisfactory yield while preserving the functional quality of the produced adsorbent.

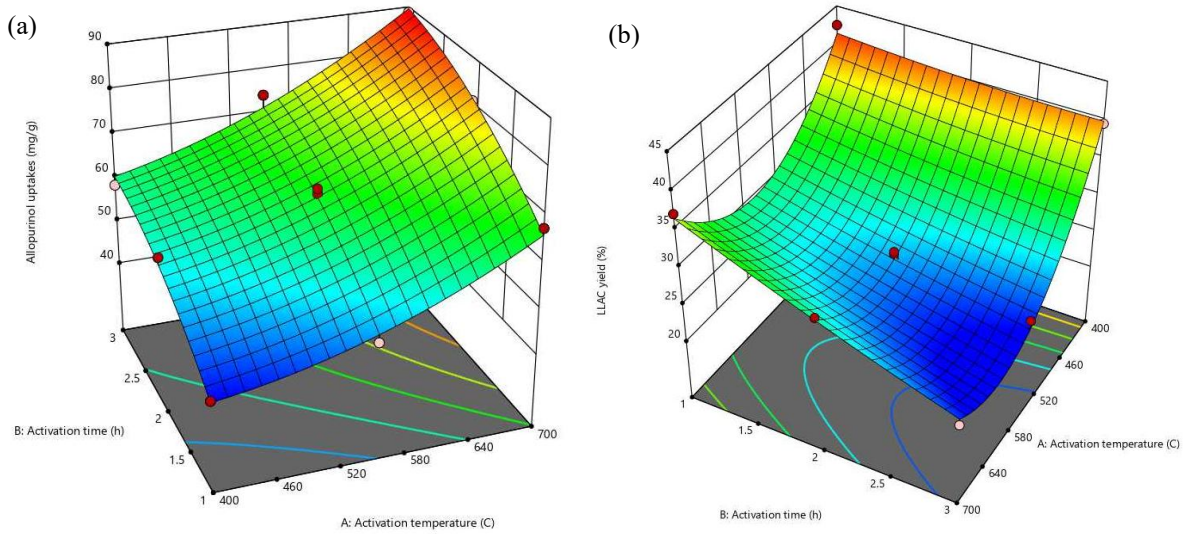


Figure 3. 3D surface plots for (a) ALLO uptake and (b) LLBAC yield responses

Optimal conditions and model validation

Table 3 presents the optimised operating parameters together with the model verification results. The optimum conditions were determined by reducing the process variables within the studied domain while achieving the highest possible responses. In the desirability function approach, the activation variables were constrained within the investigated experimental range, whereas both ALLO adsorption capacity and LLBAC yield were assigned maximization objectives. Consequently, the selected optimum condition represented a compromise solution that simultaneously considered both responses instead of focusing solely on the absolute maximum adsorption capacity. RSM optimisation identified 700 °C as the favourable activation temperature and 1.30 h as the suitable activation duration. Under these conditions, the model forecasted an ALLO adsorption capacity of 71.41 mg g^{-1} and an LLBAC yield of 34.51%. Experimental trials produced values of 73.13 mg g^{-1} and 33.76%, respectively. The small deviations between predicted and observed results, corresponding to errors of 2.35% and 2.22%, indicate strong agreement. Since the discrepancies remained well below 10%, the statistical models can be considered dependable and capable of accurate prediction [31]. The desirability value of 0.605 further indicates that the optimisation provided an acceptable overall solution within the studied experimental domain, achieving a balanced compromise between adsorption performance and LLBAC yield.

Characteristics of the samples

Surface area and pore characteristics

Table 4 summarizes the textural and pore properties of both the raw precursor and the produced LLBAC. The untreated precursor possessed an extremely limited surface area, with a BET (BET-SA) value of 2.51 m^2 g^{-1} and a total pore volume (TPV) of only 0.0001 cm^3 g^{-1}, reflecting a nearly nonporous structure. Exposure to high temperature during physical activation stimulated pore development, primarily through the breakdown of tightly bound volatile constituents, including hemicellulose and lignin fractions. Concurrently, the reaction with CO_2 promoted pore enlargement and the generation of additional voids [28]. Consequently, the LLBAC exhibited markedly enhanced porosity, reaching a BET-SA of 1152.63 m^2 g^{-1} and a mesopore surface area (MESO-SA) of 800.33 m^2 g^{-1}, together with a TPV of 0.4103 cm^3 g^{-1} and an average pore diameter (APD) of 2.08 nm, confirming the predominance of mesoporous features. These characteristics of LLBAC were found to be comparable to, or in some cases superior to, those of commercial ACs. For instance, the BET-SA of LLBAC was comparable to the commercial ACs with BET-SA values of 1248 m^2 g^{-1} [50], 1241 m^2 g^{-1} [51] and 1145 m^2 g^{-1} [52]. In contrast, other commercial ACs known as L2S, F300, and WG12 exhibited lower BET-SA values of 960, 995 and 980 m^2 g^{-1}, respectively [53]. In terms of TPV, the TPV of LLBAC was also comparable to the TPV values reported for commercial ACs of 0.4451 cm^3 g^{-1} [51] and 0.4520 cm^3 g^{-1} [53].

Elemental and proximate analysis

Table 5 compiles the results obtained from proximate and elemental evaluations of the investigated materials. Both analyses verify the successful conversion of the precursor into LLBAC through a physical activation route. The carbon fraction rose markedly from 36.11% in the untreated material to 72.36% after activation, signifying effective CO_2 gasification and the formation of a more condensed aromatic carbon network. In contrast, hydrogen declined from 6.96% to 4.33%, nitrogen from 4.45% to 2.51%, and sulfur from 0.81% to 0.45%, indicating extensive thermal decomposition and the elimination of heteroatom rich constituents. The combined oxygen and minor elements also dropped from 51.67% to 20.35%, supporting the occurrence of carbon enrichment and improved structural ordering. The proximate data follow a similar pattern. Volatile matter decreased from 58.42% to 27.56%, while fixed carbon increased substantially from 35.39% to 69.15%.

Table 3. Optimum conditions and model validation

Optimum variables		Optimum responses					
		ALLO uptake, Y_1			LLBAC yield, Y_2		
Activation temperature, X_1 (°C)	Activation time, X_2 (h)	Predicted (mg/g)	Actual (mg/g)	Error (%)	Predicted (%)	Actual (%)	Error (%)
700	1.30	71.41	73.13	2.35	34.51	33.76	2.22

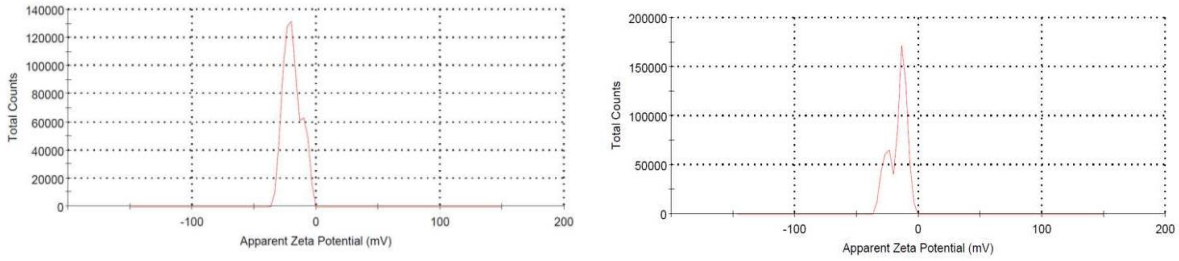
X_1 = activation temperature; X_2 = activation time

Table 4. Surface area and pore characteristics

Samples	BET-SA (m^2/g)	MESO-SA (m^2/g)	TPV (cm^2/g)	APD (nm)
Precursor	2.51	-	0.0001	-
LLBAC	1152.63	800.33	0.4103	2.08

Table 5. Elemental and proximate analysis of the samples

Samples	Elemental Analysis (%)					Proximate Analysis (%)			
	C	H	N	S	*O+	Moisture	Volatile Matter	Fixed Carbon	Ash
Precursor	36.11	6.96	4.45	0.81	51.67	4.21	58.42	35.39	1.98
LLBAC	72.36	4.33	2.51	0.45	20.35	2.11	27.56	69.15	1.18



(a) (b)

Figure 4. Zeta potential distribution for LLBAC (a) before adsorption and (b) after ALLO adsorption

The initial fixed carbon level of *Leucaena leucocephala* branches, recorded at 35.39%, exceeds many common biomasses such as rice husk, corn straw, wood dust, and coconut shell [54], which justifies its suitability as a precursor in this study. Furthermore, moisture content fell from 4.21% to 2.11%, implying greater hydrophobic character, and ash content was slightly reduced from 1.98% to 1.18%. Maintaining low ash is advantageous because mineral residues provide little adsorption capacity and can obstruct accessible pores [40].

Zeta potential analysis

Figure 4(a) and (b) illustrate the zeta potential distribution of LLBAC before and after ALLO adsorption, respectively. Prior to adsorption, LLBAC exhibited a negative zeta potential value of −19.30 mV, indicating the presence of negatively charged surface sites. The negative surface charge can be attributed to the formation of oxygen-containing functional groups during the CO_2 physical activation process, which enhanced the surface polarity and surface reactivity of the carbon material. These negatively charged sites facilitated the adsorption interaction between LLBAC and ALLO molecules. After ALLO adsorption, the zeta potential shifted from −19.30 to −16.80 mV, indicating a reduction in the negative surface charge of LLBAC. This shift suggested that ALLO molecules were successfully attached onto the adsorbent surface, partially covering or neutralizing the negatively charged active sites. The relatively small change in zeta potential further suggested that the adsorption process was predominantly governed by weak surface interactions, which was later supported by the thermodynamic findings.

Adsorption study – effect of temperature and pH

Figure 5 shows the adsorption plots for ALLO-LLBAC system at (a) different solution temperature and (b) solution pH. Based on **Figure 5(a)**, the adsorption capacity decreased slightly from 73.13 to 67.25 mg g^{-1} as the solution temperature increased from 30 to 60 °C, indicating that lower temperature favoured ALLO uptake. This trend suggests an exothermic adsorption process in which increasing thermal energy weakens the interaction between ALLO molecules and the active sites of LLBAC. At elevated temperature, enhanced molecular motion can also reduce the residence time of adsorbate molecules on the surface, leading to partial desorption. The modest decline in capacity implies that the adsorption is mainly governed by physical interactions such as van der Waals forces and pore filling rather than strong chemical bonding. Therefore, ambient temperature conditions are sufficient to achieve high ALLO removal without additional energy input.

Based on **Figure 5(b)**, solution pH strongly influenced ALLO adsorption, with the highest uptake of 73.13 mg g^{-1} observed at the original ALLO solution pH of 6.7. At acidic pH, the lower removal efficiency can be attributed to competition between excess H^+ ions and ALLO molecules for adsorption sites, which limits adsorbate attachment. As pH increased toward near neutral conditions, reduced proton competition and favourable surface interactions enhanced adsorption. Beyond neutral pH, the adsorption capacity declined markedly, reaching 27.89 mg g^{-1} at pH 12. This reduction is likely related to increased deprotonation of ALLO and possible development of negative charge on the carbon surface, which promotes electrostatic repulsion and competition with OH^- ions. Overall, near neutral pH provides the most suitable environment for ALLO adsorption onto LLBAC due to balanced electrostatic and hydrogen bonding interactions.

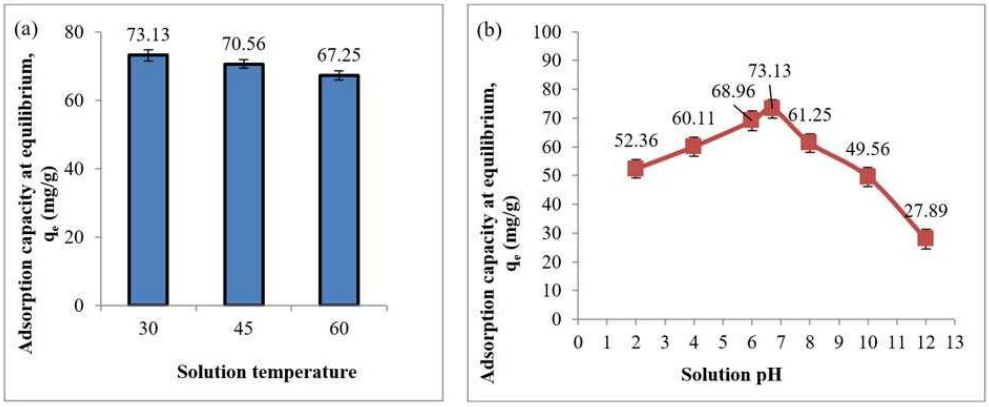


Figure 5. Adsorption plots for ALLO-LLBAC adsorption system at (a) different solution temperature and (b) different solution pH

Adsorption isotherm

Table 6 compiles the estimated parameters for the evaluated isotherm models, and the corresponding isotherm plots are illustrated in **Figure 6**. Among the examined models, the Freundlich equation described the adsorption behaviour of ALLO on LLBAC most accurately, as indicated by the smallest RMSE of 0.90 and a low relative error of 3.54%. The strong agreement with the Freundlich model suggested that adsorption occurred on a heterogeneous surface with energetically diverse adsorption sites. The Freundlich constant n_F was calculated as 1.78, which falls within the favourable range of 1 to 10 and reflects efficient affinity between ALLO molecules and the adsorbent surface. In addition, the estimated maximum uptake capacity reached 107.96 mg g^{-1}, far exceeding the reported capacity of 38.61 mg g^{-1} obtained using *Nasturtium officinale* biomass, thereby demonstrating the superior adsorption performance of LLBAC [55].

Adsorption kinetic

The kinetic behaviour of ALLO adsorption onto LLBAC at 30 °C is detailed **Figure 7**, and the kinetic parameters are given in **Table 7**. Comparison of the models shows that the PFO approach provides a more accurate description, as evidenced by its smaller average RMSE of 0.64 mg g^{-1} compared with 1.20 mg g^{-1} for the PSO model, reflecting a closer match between predicted and measured equilibrium capacities. This outcome indicates that the adsorption rate is more suitably described by PFO kinetics. Moreover, the rate constant k_1 decreased from 1.31 to 0.69 h^{-1} with rising initial ALLO concentration, suggesting that the adsorption rate slows as surface sites become progressively occupied and fewer readily accessible sites remain. Taken together, these results may suggest that physisorption plays a dominant role, where diffusion and weak intermolecular interactions contribute more significantly than chemical bond formation [56]. Nevertheless, the association of the PFO model with physisorption is not conclusive, and the actual adsorption mechanism should be further verified through thermodynamic analysis, as discussed in the subsequent section.

Table 6. Isotherm parameters for the ALLO-LLBAC adsorption system at 30 °C

Langmuir	Values	Freundlich	Values	Temkin	Values
Q_m (mg/g)	107.96	n_F	1.78	A_T (L/mg)	1.50
K_L (L/mg)	0.073	K_F (mg/g)(L/mg)$^{1/n}$	11.73	B_T (L/mg)	17.92
RMSE (mg/g)	2.26	RMSE (mg/g)	0.90	RMSE (mg/g)	5.31
Error (%)	10.19	Error (%)	3.54	Error (%)	22.21

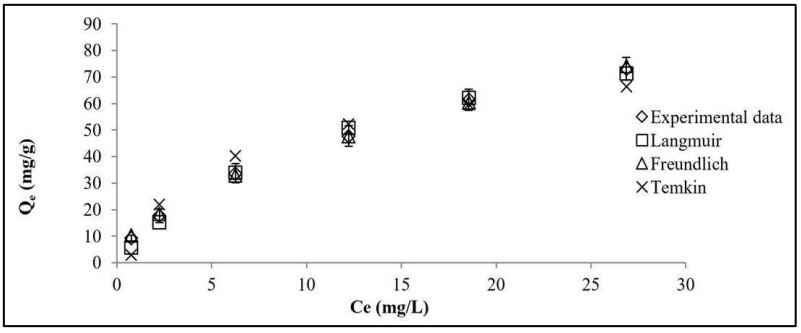


Figure 6. Isotherm plots for the ALLO-LLBAC adsorption system at 30 °C

Table 7. Kinetic parameters for the ALLO-LLBAC adsorption system at 30 °C

ALLO initial concentration (mg L^{-1})	q_e, actual (mg g^{-1}) ± SD	PFO			PSO		
		q_e, calculated (mg g^{-1})	k_1 (h^{-1})	RMSE (mg g^{-1})	q_e, calculated (mg g^{-1})	k_2 (g.$mg^{-1}h^{-1}$)	RMSE (mg g^{-1})
10	9.22 ± 0.89	9.18	1.31	0.07	10.60	0.1511	0.28
20	17.74 ± 1.59	17.85	1.11	0.17	20.97	0.0615	0.58
40	33.73 ± 2.32	34.27	1.02	0.79	40.51	0.0283	1.23
60	47.77 ± 3.52	48.17	0.84	0.56	58.83	0.0144	1.13
80	61.44 ± 3.44	62.24	0.74	0.63	77.83	0.0093	1.70
100	73.13 ± 3.67	74.98	0.69	1.60	95.25	0.0067	2.30
Average	-	-	-	0.64	-	-	1.20

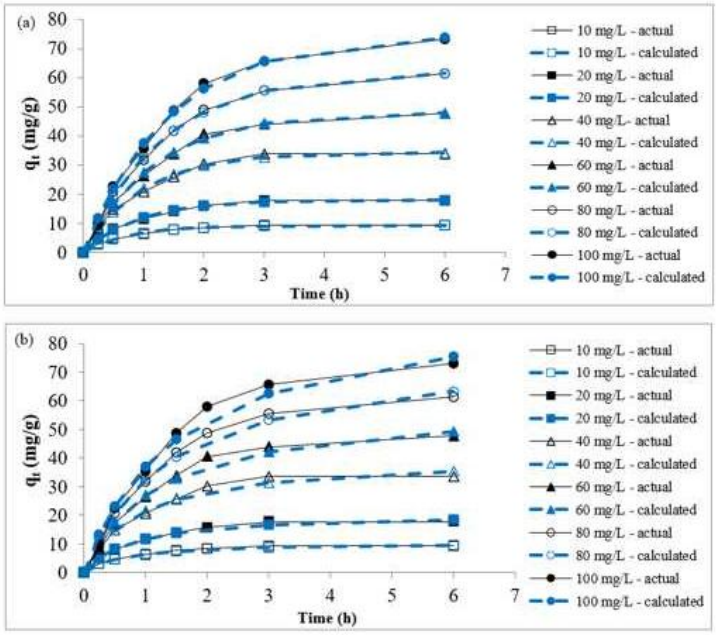


Figure 7. Kinetic plots of (a) PFO and (b) PSO for the ALLO-LLBAC adsorption system at 30 °C

Intraparticle diffusion, Boyd plot and PMT modelling

Figure 8 illustrates the intraparticle diffusion behaviour of the ALLO–LLBAC adsorption system at 30 °C, while the corresponding diffusion parameters are presented in **Table 8**. The multilinear nature of the plots suggested that the adsorption process occurred through several consecutive diffusion stages rather than a single intraparticle diffusion mechanism [42]. The first diffusion region exhibited the highest intraparticle diffusion rate constants (K_{i1}), which increased from 6.34 to 40.21 mg/g.$h^{1/2}$ as the initial ALLO concentration increased from 10 to 100 mg/L. This behaviour indicated rapid external surface adsorption caused by the stronger concentration gradient at higher ALLO concentrations. In the second region, lower K_{i2} values were obtained, reflecting the gradual diffusion of ALLO molecules into the internal pore structure of LLBAC. The third diffusion region corresponded to the equilibrium stage, where adsorption progressively slowed due to the reduced availability of active adsorption sites [57]. Furthermore, the non-zero C_i values in all regions indicated that intraparticle diffusion was not the sole rate-controlling mechanism, suggesting that boundary layer diffusion also contributed significantly to the overall adsorption process. To further verify the adsorption mechanism, Boyd plot analysis was performed and the corresponding plots are presented in Figure 9. The Boyd plots did not pass through the origin, indicating that the adsorption of ALLO molecules onto LLBAC was predominantly controlled by film diffusion rather than intraparticle diffusion [58].

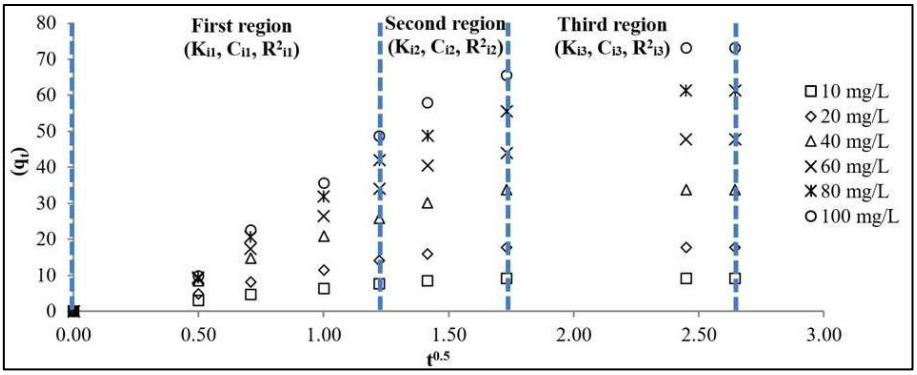


Figure 8. Intraparticle diffusion plots for the ALLO-LLBAC adsorption system at 30 °C

Table 8. Intraparticle diffusion parameters

Parameters	Initial Concentration (mg/L)					
	10	20	40	60	80	100
K_{i1} (mg/g.h$^{1/2}$)	6.34	11.67	21.45	28.15	34.89	40.21
C_{i1} (mg/g)	-0.02	-0.30	-0.73	-2.00	-3.23	-4.25
R^2_{i1}	0.9992	0.9948	0.9920	0.9789	0.9638	0.9543
K_{i2} (mg/g.h$^{1/2}$)	2.82	7.16	15.11	18.83	26.19	32.43
C_{i2} (mg/g)	4.36	5.45	7.91	12.03	10.51	10.14
R^2_{i2}	0.9834	0.9787	0.9542	0.8920	0.9762	0.9616
K_{i3} (mg/g.h$^{1/2}$)	0.0118	0.0118	0.0118	4.51	7.06	8.86
C_{i3} (mg/g)	9.19	17.71	33.70	36.22	43.36	50.45
R^2_{i3}	0.9584	0.9584	0.9584	0.9584	0.9584	0.9584

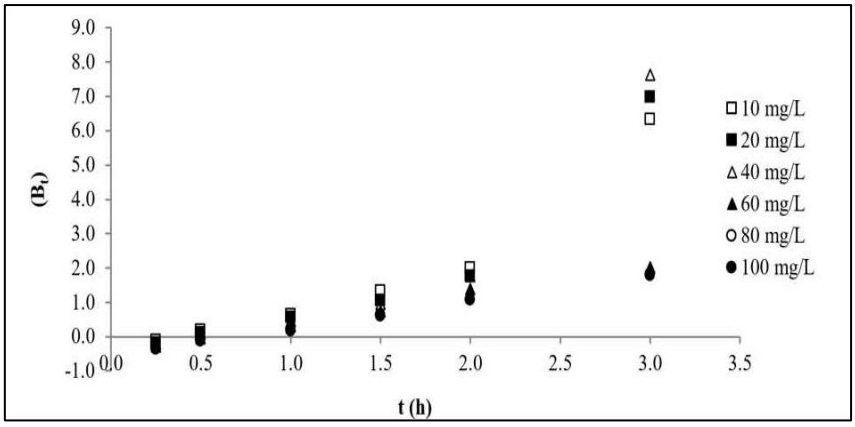


Figure 9. Boyd plots for the ALLO-LLBAC adsorption system at 30 °C

The polymath mass transfer (PMT) model was applied to further interpret the kinetic behaviour of ALLO adsorption onto LLBAC, with the PMT plot is given in **Figure 10** whilst the derived parameters are summarized in **Table 9**. The mass transfer coefficient (k_m) remained nearly constant within the range of 0.00109–0.00093 mg mL^{-1} h^{-1} for all initial ALLO concentrations, indicating minimal variation in external mass transfer resistance during adsorption. Conversely, the PMT rate constant (k_{PMT}) decreased with increasing ALLO concentration, declining from 0.30 h^{-1} at 10 mg L^{-1} to 0.0336 h^{-1} at 100 mg L^{-1}. This trend reflects a reduction in diffusion driving force as adsorption sites become progressively occupied. The low RMSE values obtained (average 0.1907 mg L^{-1}) confirm the reliability of the PMT model. In addition, the average adsorption surface area estimated by the model (733.84 m²/g) is reasonably consistent with the measured MESO-SA of 800.33 m²/g, supporting the applicability of the PMT approach, with an acceptable error of 8.31%.

Furthermore, the PMT interpretation was supported by the classical diffusion analyses discussed earlier. The intraparticle diffusion plots exhibited multilinear behaviour with non-zero intercept values, while the Boyd plots did not pass through the origin, collectively indicating that both film diffusion and pore diffusion

contributed to the overall adsorption process. These observations are consistent with the PMT findings, which similarly suggested the coexistence of external mass transfer and intraparticle diffusion mechanisms during ALLO adsorption onto LLBAC. The relatively low variation observed in the fitted PMT parameters across different ALLO concentrations further supports the stability and uniqueness of the model fitting. Moreover, the agreement between the experimentally measured MESO-SA and the PMT-estimated surface area provides additional validation for the physical assumptions employed in the PMT analysis. Although several fitted PMT parameters exhibited relatively broad 95% confidence intervals, particularly at lower ALLO concentrations, this behaviour is commonly associated with parameter interdependence in nonlinear multi-parameter regression and does not invalidate the overall mechanistic interpretation when supported collectively by the intraparticle diffusion and Boyd plot analyses. Overall, the results indicate that ALLO adsorption onto LLBAC is controlled by combined external mass transfer and pore diffusion mechanisms, with diffusion limitations becoming more pronounced at higher ALLO concentrations [59].

Adsorption thermodynamic

Figure 11 presents the thermodynamic plots for the adsorption process. From the plot shown in **Figure 11(a)**, the values of ΔH° and ΔS° were calculated as −14.91 kJ/mol and 0.030 kJ/mol·K, respectively. The negative ΔH° value indicated that the adsorption of ALLO onto LLBAC was exothermic in nature [60]. This observation was consistent with the temperature effect study, where the adsorption capacity decreased with increasing solution temperature. Meanwhile, the positive ΔS° value suggested an increase in the randomness or disorder at the solid–solution interface during the adsorption process. The ΔG°, calculated using Eq. (11), was −23.15 kJ/mol. The negative ΔG° value confirmed that the adsorption process occurred spontaneously [61]. Furthermore, Figure 11(b) was employed to estimate the E_a, which was determined to be 4.25 kJ/mol. The relatively low E_a value, which is below 42 kJ/mol indicated that the adsorption mechanism was predominantly governed by physisorption [62].

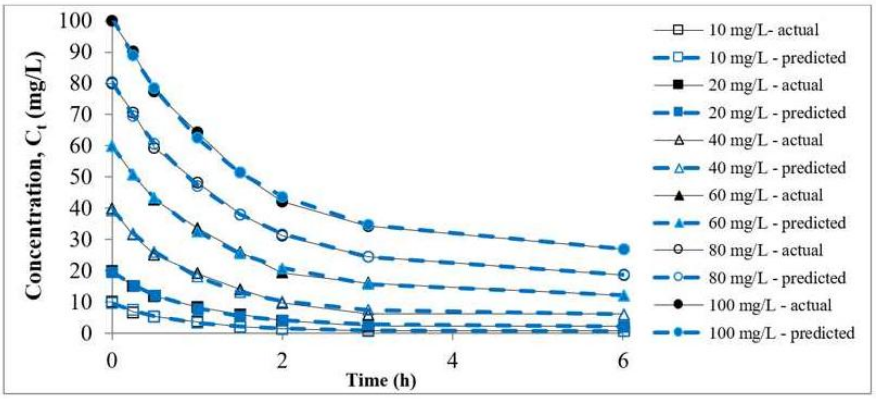


Figure 10. PMT plots for the ALLO-LLBAC adsorption system at 30 °C

Table 9. PMT parameters for the ALLO-LLBAC adsorption system at 30 °C

ALLO Initial Concentration (mg L^{-1})	C_e, Actual (mg L^{-1})	Rate Constant, k_{PMT} (h^{-1})	Mass Transfer Coefficient, k_m (mg.m.$L^{-1}h^{-1}$)	Adsorption Surface Area, a_{PMT} (m^2/g)	C_e, Calculated (mg/g)	RMSE (mg L^{-1})
10	0.78	0.44 ± 0.14	0.00284 ± 4.97 × 10^{-4}	283.59	0.77	0.0652
20	2.26	0.16 ± 3.48 × 10^{-5}	0.00108 ± 4.02 × 10^{-8}	865.91	2.18	0.1033
40	6.27	0.13 ± 0.31	0.00105 ± 3.74 × 10^{-4}	843.11	5.98	0.2347
60	12.23	0.0073 ± 1.81 × 10^{-5}	0.00092 ± 1.98 × 10^{-8}	915.03	12.01	0.2003
80	18.56	0.0501 ± 1.30 × 10^{-5}	0.00094 ± 1.72 × 10^{-8}	753.16	18.16	0.2107
100	26.87	0.0336 ± 0.0050	0.00093 ± 6.76 × 10^{-6}	742.25	26.10	0.3297
Average	-	-	-	*733.84*	-	*0.1907*

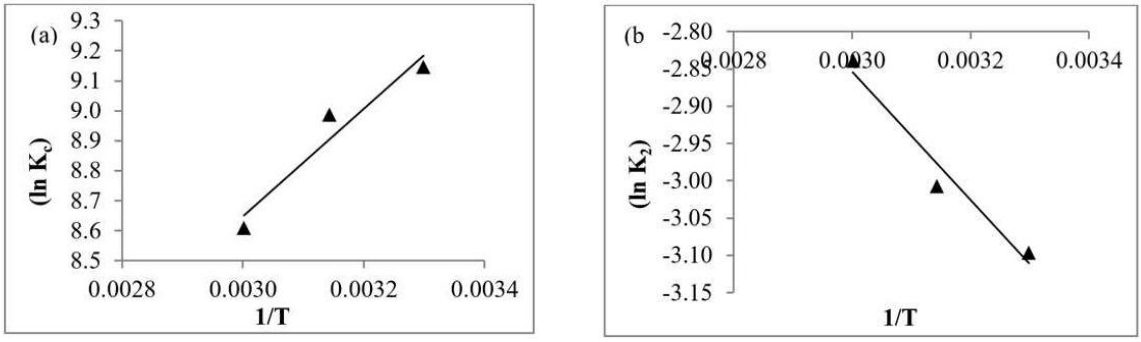


Figure 11. Thermodynamic plots of (a) ln K_L versus 1/T and (b) ln K_2 versus 1/T

Table 10. Adsorption uptakes of ALLO and other components in multicomponent system

	Adsorption Uptake (mg/g)				
	Single Component	**Binary with PARA**	**Binary with NO^{3-}**	**Binary with Pb^{2+}**	**Quaternary System (Simulated Real Hospital wastewater)**
ALLO	73.13 ± 3.16	64.21 ± 3.15	70.86 ± 3.35	60.21 ± 3.11	60.09 ± 3.02
PARA	52.69 ± 3.38	42.08 ± 3.29	-	-	41.07 ± 3.45
NO^{3-}	23.78 ± 3.26	-	14.59 ± 3.65	-	9.12 ± 3.24
Pb^{2+}	86.24 ± 3.75	-	-	68.65 ± 3.24	71.24 ± 3.27

Adsorption in multicomponent system

Table 10 shows the adsorption uptake of ALLO, paracetamol (PARA), nitrate (NO_3^-) and Pb^{2+} ions in single, binary and quaternary systems using LLBAC as the adsorbent. In the single-component system, Pb^{2+} exhibited the highest adsorption capacity of 86.24 mg/g, followed by ALLO, PARA and NO_3^-. However, the adsorption capacities of all components decreased in the multicomponent systems due to competitive adsorption for the limited active sites available on the adsorbent surface. The negatively charged surface of LLBAC, reflected by its zeta potential value of −19.30 mV, likely favoured the adsorption of Pb^{2+} through electrostatic attraction. In contrast, the adsorption of NO_3^- remained relatively low, which may be attributed to electrostatic repulsion between the negatively charged adsorbent surface and the anionic nitrate species. Among the binary systems, the presence of Pb^{2+} caused the greatest reduction in ALLO uptake, suggesting stronger competition between Pb^{2+} and ALLO for the available adsorption sites. In the quaternary system simulating real hospital wastewater, LLBAC still demonstrated satisfactory simultaneous removal capability toward both organic and inorganic contaminants under competitive adsorption conditions.

Regeneration study

Figure 12 shows the regeneration plots for ALLO-LLBAC adsorption system. The regeneration study of spent LLBAC was performed through physical reactivation using the optimum preparation condition determined by RSM, namely an activation temperature of 700 °C and activation duration of 1.30 h. After each adsorption cycle, the used LLBAC was recovered, dried, and subjected to thermal reactivation prior to reuse under identical adsorption conditions. Fresh LLBAC (cycle 0) exhibited the highest ALLO uptake of 73.13 mg/g with 100% adsorbent yield. Following the first regeneration cycle, the adsorption capacity decreased slightly to 65.25 mg/g, corresponding to approximately 89.2% retention of the original adsorption performance.

However, further regeneration cycles gradually reduced both the ALLO uptake and LLBAC yield. By the fifth regeneration cycle, the adsorption capacity declined to 9.25 mg/g, while the adsorbent yield decreased to 19.17 mg/g. The progressive decline in adsorption performance may be attributed to partial pore collapse, blockage of active sites by residual ALLO molecules, and gradual deterioration of surface functional groups during repeated high-temperature regeneration processes. In addition, the reduction in LLBAC yield suggests carbon burn-off and material loss during repeated thermal treatment. Nevertheless, the regenerated LLBAC maintained relatively acceptable adsorption capability up to the second regeneration cycle, indicating that the adsorbent possesses moderate regeneration potential for short-term reuse applications.

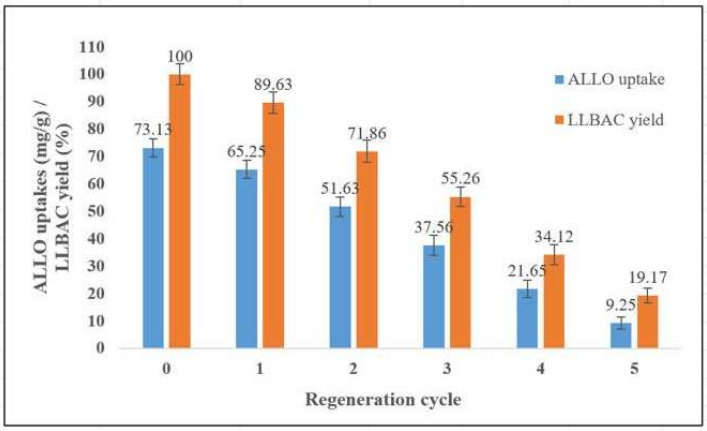


Figure 12. Regeneration plots for ALLO-LLBAC adsorption system

Conclusion

LLBAC was effectively produced through a one-step CO_2 activation process and exhibited notable capability for eliminating ALLO from water. Statistical optimisation using RSM revealed that activation temperature exerted the greatest influence on both adsorption performance and carbon yield, with the most favourable preparation conditions found at 700 °C and 1.30 h. Isotherm assessment indicated that ALLO uptake conformed to the Freundlich equation, reflecting multilayer adsorption on a heterogenous surface, and delivering a maximum capacity, Q_m of 107.96 mg g^{-1}. Kinetic results were more accurately represented by the PFO model, pointing to a mechanism largely governed by physical interactions and diffusion related transport. Results from PMT simulation aligned with these findings by producing stable mass transfer parameters and close correspondence between calculated and measured surface areas. Taken together, the optimisation outcomes, equilibrium behaviour, kinetic trends, and mass transfer evaluation demonstrate that LLBAC functions as a cost effective and promising adsorbent for the purification of ALLO polluted water.

Acknowledgement

This research is supported by Malaysian Ministry of Higher Education under the Prototype Research Grant Scheme (project code: PRGS/1/2025/TK/USM/01/1)

References

1. Zaini, Y. M. M., Purba, L. D. A., Abdullah, N., Yuzir, A., Iwamoto, K., and Mohamad, S. E. (2022). Removals of atenolol, gliclazide and prazosin using sequencing batch reactor. *Materials Today: Proceedings,* 65: 3007-3014.
2. Mohamad, F. M. Y., Abdullah, A. Z., and Ahmad, M. A. (2024). Amoxicillin adsorption from aqueous solution by Cu(II) modified lemon peel based activated carbon: Mass transfer simulation, surface area prediction and F-test on isotherm and kinetic models. *Powder Technology,* 438: 119589.
3. Gartenberg, A., Winkel, M., and Leonard, N. (2024). Spontaneous tumor lysis syndrome in a patient with chronic myeloid leukemia treated successfully with allopurinol. *American Journal of Emergency Medicine,* 78: 242.e1-242.e3.
4. Pol, K. H. v. d., Wever, K. E., Verbakel, M., Visseren, F. L. J., Cornel, J. H., and Rongen, G. A. (2021). Allopurinol to reduce cardiovascular morbidity and mortality: A systematic review and meta-analysis. *PLoS ONE,* 16(12): 1-19.
5. Saadh, M. J., Mirzaei, M., Ghnim, Z. S., Mosaddad, S. A., and Salem-Bekhit, M. M. (2024). Density functional theory analyses of an iron-doped nanocage for the adsorption of allopurinol drug towards the development of novel carriers. *Computational and Theoretical Chemistry,* 1237: 114664.
6. Funke, J., Prasse, C., Lütke Eversloh, C., and Ternes, T. A. (2015). Oxypurinol – A novel marker for wastewater contamination of the aquatic environment. *Water Research,* 74: 257-265.
7. Stamp, L. K., and Chapman, P. T. (2020). Allopurinol hypersensitivity: Pathogenesis and prevention. *Best Practice and Research: Clinical Rheumatology,* 34(4).
8. Hali, F., Chagraoui, H., Meftah, A., Marnissi, F., Chaabi, S., Chiheb, S., and Filali, H. (2023). Allopurinol induced severe cutaneous adverse reactions: Vigilance of prescription (31 cases). *Revue Francaise d'Allergologie,* 63(2).
9. Khir, N. H. M., Salleh, N. F. M., Ghafar, N. A., Shukri, N. M., and Jusoh, R. (2025). Preparation and characterization of modified rambutan peels for the removal of chromium(VI) and nickel(II) from aqueous solution: Environmental impact and optimization *Malaysian Journal of Analytical Sciences,* 29(1): 1292.
10. Firdaus, M. Y. M., Mohd Johan Jaya, E., and Ahmad, M. A. (2022). Single-stage microwave assisted coconut shell based activated carbon for removal of Zn(II) ions from aqueous solution – Optimization and batch studies. *Arabian Journal of Chemistry,* 15: 104011.

11. Yusop, M. F. M., Rashid, M. M., Alam, M. M., and Ahmad, M. A. (2026). Cu^{2+}-surface-modified activated carbon from nutshells for enhanced metformin removal: Mass transfer simulation, attraction mechanism and F-test studies. *Water, Air, & Soil Pollution,* 237(9): 518.
12. Chen, J., Li, L., Shi, G., Yan, Y., Wang, Q., Yu, Z., Yan, L., and Yu, Y. (2025). Adsorption of chlorinated hydrocarbons by different kinds of soils: Kinetics, influencing factors, mechanism. *Journal of Hazardous Materials Advances,* 18: 100638.
13. Ramlee, D. A., Nordin, N. A., Rahman, N. A., and Bahruji, H. (2024). Removal of acetaminophen by using electrospun pan/sago lignin-based activated carbon nanofibers. *Malaysian Journal of Analytical Sciences,* 28(6): 1442 - 1457.
14. Gunasekaran, S., Liu, A. J. X., and Ng, S. L. (2024). Activated carbon/iron oxide composites with different weight ratios for acid orange 7 removal. *Malaysian Journal of Analytical Sciences,* 28(6): 1359 - 1373.
15. Mohamad, F. M. Y., Tamar Jaya, M. A., Idris, I., Abdullah, A. Z., and Ahmad, M. A. (2023). Optimization and mass transfer simulation of remazol brilliant blue R dye adsorption onto meranti wood based activated carbon. *Arabian Journal of Chemistry,* 16: 104683.
16. Ahammad, N. A., Yusop, M. F. M., Mohd Din, A. T., and Ahmad, M. A. (2021). Preparation of alpinia galanga stem based activated carbon via single-step microwave irradiation for cationic dye removal. *Sains Malaysiana,* 50(8): 2251-2269.
17. Ahmad, M. A., Yusop, M. F. M., Awang, S., Yahaya, N. K. E. M., Rasyid, M. A., and Hassan, H. (2021). Carbonization of sludge biomass of water treatment plant using continuous screw type conveyer pyrolyzer for methylene blue removal. *IOP Conference Series: Earth and Environmental Science,* 765: 012112.
18. Nasran, N. K. M., Firdaus, M. Y. M., Faizal, P. M. L. M., and Azmier, A. M. (2023). Alteration of Tecoma chip wood waste into microwave-irradiated activated carbon for amoxicillin removal: Optimization and batch studies. *Arabian Journal of Chemistry,* 16(10): 105110.
19. Kato-Noguchi, H., and Kurniadie, D. (2022). Allelopathy and Allelochemicals of Leucaenaleucocephala as an Invasive Plant Species. *Plants,* 11(13): 1672.
20. Badalamenti, E., Pasta, S., Sala, G., Catania, V., Quatrini, P., and La Mantia, T. J. I. J. o. P. B. (2020). The paradox of the alien plant *Leucaena leucocephala* subsp. glabrata (Rose) S. Zárate in Sicily: another threat for the native flora or a valuable resource? *International Journal of Plant Biology,* 11(1).
21. Sophia A, C., and Lima, E. C. (2018). Removal of emerging contaminants from the environment by adsorption. *Ecotoxicology and Environmental Safety,* 150: 1-17.
22. Perera, A. A. P. R., Madhushani, K. A. U., Kumar, A., and Gupta, R. K. (2023). Metal-organic frameworks for wastewater treatment: Recent developments, challenges, and future prospects. *Chemosphere,* 339: 139713.
23. Ranjan Rout, D., and Mohan Jena, H. (2022). Synthesis of novel reduced graphene oxide decorated β-cyclodextrin epichlorohydrin composite and its application for Cr(VI) removal: Batch and fixed-bed studies. *Separation and Purification Technology,* 278.
24. Rout, D. R., Jena, H. M., Baigenzhenov, O., and Hosseini-Bandegharaei, A. (2023). Graphene-based materials for effective adsorption of organic and inorganic pollutants: A critical and comprehensive review. *Science of The Total Environment,* 863: 160871.
25. Capodaglio, A. G., Bojanowska-Czajka, A., and Trojanowicz, M. (2018). Comparison of different advanced degradation processes for the removal of the pharmaceutical compounds diclofenac and carbamazepine from liquid solutions. *Environmental Science and Pollution Research,* 25(28): 27704-27723.
26. Taoufik, N., Boumya, W., Achak, M., Sillanpää, M., and Barka, N. (2021). Comparative overview of advanced oxidation processes and biological approaches for the removal pharmaceuticals. *Journal of Environmental Management,* 288: 112404.
27. Obotey Ezugbe, E., and Rathilal, S. (2020). Membrane technologies in wastewater treatment: A review. *Membranes (Basel),* 10(5): 89.
28. Firdaus, M. Y. M., Rashid, M. M., Alam, M. M., and Ahmad, M. A. (2025). Enhanced Cd^{2+} removal via deprotonated-mango trunk functionalized carbon: Optimization and F-test for linear and non-linear isotherm and kinetic models. *Chemical Engineering Research and Design,* 220: 96-116.
29. Daouda, M. M. A., Akowanou, A. V. O., Mahunon, S. E. R., Adjinda, C. K., Aina, M. P., and Drogui, P. (2021). Optimal removal of diclofenac and amoxicillin by activated carbon prepared from coconut shell through response surface methodology. *South African Journal of Chemical Engineering,* 38(1): 78-89.
30. Yusop, M. F. M., Baharudin, M. H., Rashid, M. M., Alam, M. M., and Ahmad, M. A. (2025). Amoxicillin adsorption onto oil palm trunk-derived activated carbon: synthesis optimization, modelling of mass transfer and ultrasonic regeneration. *Journal of Chemical Technology & Biotechnology,* 100(6): 1310-1327.

31. Yusop, M. F. M., Mohd Johan Jaya, E., Mohd Din, A. T., Bello, O. S., and Ahmad, M. A. (2022). Single-stage optimized microwave-induced activated carbon from coconut shell for cadmium adsorption. *Chemical Engineering & Technology,* 45(11): 1943-1951.
32. Angel, L., Villot, A., Rodriguez Susa, M., Plazas-Tuttle, J., Andres, Y., and Gerente, C. (2025). Optimizing activated carbon production from chontaduro seeds via physical activation with steam for ibuprofen removal: A factorial design and multi-attribute utility theory approach. *Journal of Water Process Engineering,* 70: 107020.
33. Mirzaee, S. A., Bayati, B., Valizadeh, M. R., Gomes, H. T., and Noorimotlagh, Z. (2021). Adsorption of diclofenac on mesoporous activated carbons: Physical and chemical activation, modeling with genetic programming and molecular dynamic simulation. *Chemical Engineering Research and Design,* 167: 116-128.
34. Inglezakis, V. J., Balsamo, M., and Montagnaro, F. (2020). Liquid–solid mass transfer in adsorption systems—an overlooked resistance? *Industrial & Engineering Chemistry Research,* 59(50): 22007-22016.
35. Mohd Ramli, M. R., Shoparwe, N. F., and Ahmad, M. A. (2023). Methylene blue removal using activated carbon adsorbent from Jengkol peel: Kinetic and mass transfer studies. *Arabian Journal for Science and Engineering,* 48(7): 8585-8594.
36. Firdaus, M. Y. M., Rashid, M. M., Alam, M. M., and Ahmad, M. A. (2026). Copper-modified surface of orange peel-derived activated carbon for amoxicillin removal: mass transfer simulation, attraction mechanism, and regeneration studies. *Arabian Journal for Science and Engineering,* 51: 13839–13861.
37. Langmuir, I. (1918). The adsorption of gases on plane surfaces of glass, mica and platinum. *Journal of the American Chemical Society,* 40(9): 1361-1403.
38. Freundlich, H. (1906). Over the adsorption in solution. *Journal of Physical Chemistry,* 57(385471): 1100-1107.
39. Tempkin, M., and Pyzhev, V. (1940). Kinetics of ammonia synthesis on promoted iron catalyst. *Acta Physicochimica URSS,* 12(1): 327.
40. Firdaus, M. Y. M., Rashid, M. M., Alam, M. M., and Ahmad, M. A. (2025). Synthesis of deprotonated grape stem functionalized carbon for boosted Cu^{2+} adsorption – optimization, interaction mechanism, and F-test analysis. *Microchemical Journal,* 218: 115795.
41. Revellame, E. D., Fortela, D. L., Sharp, W., Hernandez, R., and Zappi, M. E. (2020). Adsorption kinetic modeling using pseudo-first order and pseudo-second order rate laws: A review. *Cleaner Engineering and Technology,* 1: 100032.
42. Mohamad, F. M. Y., Rashid, M. M., Alam, M. M., and Ahmad, M. A. (2026). Synthesis of deprotonated-langsat peel activated carbon for improved Pb^{2+} adsorption: Optimization and F-test for isotherm and kinetic models. *Diamond and Related Materials,* 165: 113650.
43. Weber, W. J., and Morris, J. C. (1963). Kinetics of adsorption on carbon from solution. *Journal of the Sanitary Engineering Division,* 89(2): 31-59.
44. Boyd, G. E., Adamson, A. W., and Myers, L. S., Jr. (1947). The exchange adsorption of ions from aqueous solutions by organic zeolites. II. Kinetics. *Journal of the American Chemical Society,* 69(11): 2836-2848.
45. Lima, E. C., Hosseini-Bandegharaei, A., Moreno-Piraján, J. C., and Anastopoulos, I. (2019). A critical review of the estimation of the thermodynamic parameters on adsorption equilibria. Wrong use of equilibrium constant in the Van't Hoof equation for calculation of thermodynamic parameters of adsorption. *Journal of Molecular Liquids,* 273: 425-434.
46. Beyan, S. M., Prabhu, S. V., Sissay, T. T., and Getahun, A. A. (2021). Sugarcane bagasse based activated carbon preparation and its adsorption efficacy on removal of BOD and COD from textile effluents: RSM based modeling, optimization and kinetic aspects. *Bioresource Technology Reports,* 14: 100664.
47. Mahari, W. A. W., Zainuddin, N. F., Nik, W. M. N. W., Chong, C. T., and Lam, S. S. (2016). Pyrolysis recovery of waste shipping oil using microwave heating. *Energies,* 9(10): 780.
48. Weldekidan, H., Patel, H., Mohanty, A., and Misra, M. (2024). Synthesis of porous and activated carbon from lemon peel waste for CO2 adsorption. *Carbon Capture Science & Technology,* 10: 100149.
49. Mohamad, F. M. Y., Rashid, M. M., Alam, M. M., and Ahmad, M. A. (2025). Copper metal-functionalized carbon from rattan waste via microwave pyrolysis for enhanced chloramphenicol removal: Optimization and F-test study. *Particuology,* 100: 196-213.
50. Nguyen, D. T., Tran, H. N., Juang, R.-S., Dat, N. D., Tomul, F., Ivanets, A., Woo, S. H., Hosseini-Bandegharaei, A., Nguyen, V. P., . . . Chao, H.-P. (2020). Adsorption process and mechanism of acetaminophen onto commercial activated carbon. *Journal of Environmental Chemical Engineering,* 8(6): 104408.
51. Shahrokhi-Shahraki, R., Benally, C., El-Din, M. G., and Park, J. (2021). High efficiency removal of heavy metals using tire-derived activated carbon vs commercial activated carbon: Insights into the adsorption mechanisms. *Chemosphere,* 264: 128455.

52. Sun, Y., Wang, Z., Zhang, S., Liu, C., and Xu, Y. (2024). Preparation of composites with MgAl-LDH-modified commercial activated carbon for the quick removal of Cr(VI) from aqueous solutions. *Environmental Science and Pollution Research,* 31(28): 41032-41045.
53. Kuśmierek, K., Dąbek, L., and Świątkowski, A. (2025). The influence of the shape and grain size of commercial activated carbons on their sorption efficiency towards organic water pollutants. *Desalination and Water Treatment,* 321: 100996.
54. Wei, X., Huang, S., Yang, J., Liu, P., Li, X., Wu, Y., and Wu, S. (2023). Adsorption of phenol from aqueous solution on activated carbons prepared from antibiotic mycelial residues and traditional biomass. *Fuel Processing Technology,* 242: 107663.
55. Veysi, O., Elif, O., Davut, B., and Ahmet, O. (2010). Simultaneous removal of indomethacine, papaverine and allopurinol from aqueous solution by using submerged aquatic plant *Nasturtium officinale*. *Asian Journal of Chemistry,* 22(3): 2081-2089.
56. Wang, J., and Guo, X. (2023). Adsorption kinetics and isotherm models of heavy metals by various adsorbents: An overview. *Critical Reviews in Environmental Science and Technology,* 53(21): 1837-1865.
57. Aziz, A., Mohamad Yusop, M. F., and Ahmad, M. A. (2024). Harnessing microwave energy to transform *Nephelium lappaceum* L. peel into activated carbon for chloramphenicol eradication in aqueous solutions. *Materials Chemistry and Physics,* 318: 129311.
58. Yusop, M. F. M., Rashid, M. M., Alam, M. M., and Ahmad, M. A. (2026). Optimized copper-functionalized carbon from *Lansium parasiticum* trunk for chloramphenicol removal from aqueous solution. *International Journal of Environmental Science and Technology,* 23(4): 306.
59. Mohamad, F. M. Y., Abdullah, A. Z., and Ahmad, M. A. (2023). Adsorption of remazol brilliant blue R dye onto jackfruit peel based activated carbon: Optimization and simulation for mass transfer and surface area prediction. *Inorganic Chemistry Communications,* 158: 111721.
60. Yusop, M. F. M., Ahmada, M. A., Roslia, N. A., Gonawana, F. N., and Abdullahb, S. J. (2021). Scavenging malachite green dye from aqueous solution using durian peel based activated carbon. *Malaysian Journal of Fundamental and Applied Sciences,* 17(1): 95-103.
61. El Jery, A., Alawamleh, H. S. K., Sami, M. H., Abbas, H. A., Sammen, S. S., Ahsan, A., Imteaz, M. A., Shanableh, A., Shafiquzzaman, M., and Al-Ansari, N. (2024). Isotherms, kinetics and thermodynamic mechanism of methylene blue dye adsorption on synthesized activated carbon. *Scientific Reports,* 14(1): 970.
62. Firdaus, M. Y. M., Nasehir Khan, M. N., Zakaria, R., Abdullah, A. Z., and Ahmad, M. A. Mass transfer simulation on remazol brilliant blue R dye adsorption by optimized teak wood based activated carbon. *Arabian Journal of Chemistry,* 16: 104780.